Research on the relationship between temperature field and thermal damage in a multidimensional heat transfer model of multi-layered skin tissue

Penghui Wang(王鹏辉)[1], Xiao Gao(高霄)[1], Xiang Li(李响)[1], Yuqing Ren(任妤晴)[1], Jie Liu(刘杰)[1], Ziyi Zhen(甄子怡)[1], Hui Cao(曹辉)[1,†], and Na Cao(曹娜)[2,‡]

[1] *School of Physics and Information Technology, Shaanxi Normal University, Xian* 710119, *China*
[2] *School of Physical Science and Technology, Inner Mongolia University, Neimenggu* 010021, *China*

(Received 12 January 2026; revised manuscript received 24 February 2026; accepted manuscript online 11 March 2026)

Laser therapy is widely used in clinical applications such as dermatological treatments and local tumor ablation due to its non-invasiveness, controllable energy deposition, and strong spatial selectivity. Although theoretical models based on bioheat transfer and the Arrhenius damage criterion are well-established, several key issues remain unclear in quantitative prediction and model simplification. These include the relative contributions of temperature-dependent thermophysical parameters, the impact of lateral heat diffusion on damage extent, and the coupling mechanism between temperature dependence and model dimensionality (1D/2D). To address the aforementioned issues, a controlled computing framework is established in which dimensional (1D/2D) configurations and temperature-dependent treatments of thermophysical parameters with three-layered skin tissue as the research object. This framework is employed for systematic analysis of the spatiotemporal evolution of temperature fields and Arrhenius thermal damage, with the two-dimensional lateral damage width used to characterize the damage range. The research results indicate that temperature dependence of thermal conductivity is the dominant factor affecting the accuracy of thermal damage prediction in both 1D and 2D models. Neglecting thermal conductivity can lead to overestimation of lateral damage width by up to 0.2 mm and an advance of critical damage time by approximately 0.1 s in two-dimensional simulations. Besides, lateral heat diffusion in 2D calculations significantly amplifies errors in damage extent and critical time which stem from the assumption of constant thermal conductivity, and which further reveal the coupling between temperature dependence and dimensionality effects. This paper provides a theoretical foundation for parameter sensitivity analysis and uncertainty control in laser therapy damage prediction.

Keywords: bioheat transfer, dual-phase lag model, thermal damage, temperature dependence, parameter sensitivity

PACS: 87.50.wp, 87.19.xb, 44.05.+e

DOI: 10.1088/1674-1056/ae5051 **CSTR:** 32038.14.CPB.ae5051

1. Introduction

With the advancement of precision medicine, laser thermotherapy is gaining increasing importance in clinical applications such as dermatological treatments and local tumor ablation. From the perspective of energy transport, its therapeutic effect and safety depend on localized energy deposition generated by the selective photothermal effect and the resulting temperature field evolution. This requires that during the treatment process sufficient and controllable temperature elevation is achieved in the target area, while limiting heat diffusion and heat redistribution to prevent unintended expansion of the damage range in non-target areas.[1,2] The formation of tissue thermal damage can be understood as a process in which energy deposition first determines the heat source distribution. This distribution is then converted into spatiotemporal temperature variations through heat transfer. Ultimately, thermal damage accumulation is evaluated based on the temperature history using damage kinetic criteria. This means that the accuracy of temperature field prediction directly affects the determination of the damage threshold, the estimation of the damage range, and the determination of the safety boundary. Therefore, improving the reliability of thermal injury prediction has become a research consensus in this field. Its key support lies in the reasonable characterization of the bioheat transfer model for transient temperature fields and the credible representation of tissue thermophysical properties.[3] Based on the aforementioned key elements, establishing a thermal injury prediction system oriented towards clinical hyperthermia and applicable for risk assessment remains a core issue continuously focused on in current research.

Thermal property parameters of skin tissue are not uniform constants at the level of temperature field modeling. Parameters such as thermal conductivity, specific heat, and blood perfusion rate differ significantly between the epidermis, dermis, and subcutaneous tissue, and also vary with individuals and physiological states.[3] This makes the model highly sen-

†Corresponding author. E-mail: caohui@snnu.edu.cn
‡Corresponding author. E-mail: caona@imu.edu.cn

© 2026 Chinese Physical Society and IOP Publishing Ltd. All rights, including for text and data mining, AI training, and similar technologies, are reserved.

CPB Online First Press

sitive to parameter selection and handling of interlayer interfaces. Under short-pulse or high-power laser heating conditions, when the heating time scale is comparable to the characteristic thermal response time of biological tissue, heat flux tends to exhibit lagging and finite propagation characteristics during temperature gradient formation. This imposes constraints on the applicability of the instantaneous response assumption in classical Fourier heat conduction theory.[4,5] To characterize such heat transfer features, the dual-phase lag (DPL) model was proposed by Tzou *et al*. They introduced heat flux relaxation time and temperature gradient relaxation time in the macroscopic equation to describe the phase lag effect between heat flux and temperature gradient.[6–9] Consequently, the DPL model is often used for transient heat transfer calculations in laser-tissue interactions, and provides a more comprehensive description of transient temperature response during short-time heating compared to the classic Pennes bioheat equation.[10–12] However, when conducting practical modeling for quantitative prediction of thermal damage, it is often necessary to consider both the trade-offs in model dimensions and the handling of temperature dependence in thermophysical parameters. Existing studies have shown that thermophysical parameters of biological tissues such as thermal conductivity and specific heat are not constant during heating, and often exhibit significant nonlinear changes.[13,14] Bhattacharya *et al.* experimentally characterized the temperature response of thermal conductivity.[15] Lopresto *et al.* pointed out that the temperature dependence of thermophysical parameters can alter model output and introduce considerable prediction bias.[16] Valvano *et al.* emphasized the influence of such nonlinear parameters on transient heat transport during short-time laser heating of layered tissues.[17] Furthermore, Vanni *et al.* provided supporting experimental evidence from *ex vivo* biological tissues and other materials.[16] Regarding temperature dependence of parameters such as specific heat, Wang *et al.* conducted multiple measurements and developed parametric models.[18,19] Therefore, when quantitative prediction of thermal damage is required, it is equally critical to not only select appropriate heat transfer models but also to reasonably handle the temperature dependence of thermal property parameters. How these parameters are managed will directly affect the quantitative assessment of their impact.

Although existing studies have confirmed that temperature dependence of thermophysical parameters can change predictions of temperature fields and thermal damage,[17,19–22] systematic quantitative conclusions under unified conditions are still lacking for quantitative prediction and evaluation of model simplification. First, a consistent comparison and ranking of the relative contributions of temperature dependence of different thermophysical parameters to prediction bias have not been formed, making it difficult to provide a clear basis for parameter selection in simplified models. Second, due to computational costs and modeling complexity, many studies still adopt 1D approximations or conduct validation under constrained conditions. This has led to the influence magnitude of lateral heat diffusion on temperature distribution and damage range in multi-dimensional scenarios, as well as the model bias introduced thereby, not being systematically evaluated.[21–23] Third, under multidimensional heat transfer conditions, the relationship between coupling effects of temperature-dependent parameter treatment and model dimensionality remains unclear. In summary, resolving the coupling mechanism between temperature dependence and model dimensionality remains an area that existing research has yet to systematically address. Based on the above issues, we establish one-dimensional (1D) and two-dimensional (2D) numerical models based on a dual-phase-lag heat conduction model, focusing on temperature dependence and model dimensions. These models are employed to solve the spatiotemporal evolution of temperature fields and thermal damage during laser irradiation. Both numerical models take three-layer biological tissue as the research subject, and calculate thermal damage via the Arrhenius damage criterion on the basis of unified configurations of the laser heat source and boundary conditions. The core work of this paper consists of the following aspects. To begin with, a control-variable comparative design is employed to either consider or neglect the temperature dependence of thermophysical property inputs for relevant parameters such as thermal conductivity and volumetric heat capacity. This allows for a quantitative comparison of their impacts on thermal damage prediction and provides a ranking of their relative contributions, which offers a basis for simplifying parameter selection in models. Subsequently, by incorporating lateral heat diffusion into the 2D model, the magnitude of its effects on key quantities such as temperature distribution and damage extent is evaluated and compared with the results from 1D approximations. Finally, a systematic comparison is conducted within both 1D and 2D frameworks to assess the predictive deviations resulting from different simplification assumptions, thereby characterizing the coupled influence of thermophysical property temperature dependence and model dimensionality. The results of this paper provide a quantitative basis for parameter optimization, model simplification, and definition of their applicable scopes in laser thermotherapy.

2. Theoretical model and method

2.1. Three-layered skin model and volumetric heat source

Based on skin anatomy, the skin in the study area is divided into three layers, which are the epidermis, the dermis and the subcutaneous tissue (Figs. 1 and 2). Each layer has uniform thickness and is assumed isotropic, with an initial

CPB Online In-Press

temperature $T_0 = 37$ °C.[24] To accurately simulate laser energy deposition in multi-layered skin tissue, GPU-accelerated Monte Carlo simulation (MCX) is used to model photon transport within tissue. This method obtains the 3D spatial light power density distribution, which serves as heat source input for subsequent heat conduction models.[25–28] Model parameters are set according to optical properties of typical Asian skin (Fitzpatrick III/IV type) to ensure physiological realism (Fig. 3). Laser beams irradiate the skin surface vertically, and energy distribution on the incident surface is described by a Gaussian beam. Under identical source parameters, the Monte Carlo light transport simulation yields the fluence rate distribution $\phi(r)$. Here, $\boldsymbol{r}$ is the spatial position vector. For the 1D model, $r = z$; for the 2D model, $\boldsymbol{r} = (y,z)$. According to the absorption law, the absorbed power density per unit volume is

$$A(r) = \mu_{\mathrm{a}} f(r),$$

where μ_{a} is the absorption coefficient. For a short-pulse laser with a temporal profile $P(t)$, the volumetric heat source is expressed as

$$Q(\boldsymbol{r},t) = \mu_{\mathrm{a}} f(\boldsymbol{r}) P(t).$$

Here, $Q(\boldsymbol{r},t)$ represents the power density representing the rate of heat generation per unit volume. Optical input parameters for each layer are listed in Table 1.

Table 1. Required optical parameters for each layer of skin tissue.[29–33]

	Thickness (mm)	Absorption coefficient (mm^{-1})	Scattering coefficient (mm^{-1})	Anisotropy factor	Refractive index
Epidermis	0.1	0.14	13	0.85	1.33
Dermis	1.5	0.01	7.35	0.9	1.4
Subcutaneous tissue	4.4	0.003	5	0.7	1.4

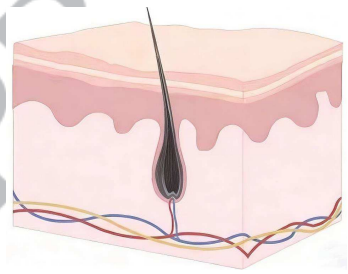


Fig. 1. Skin tissue model.

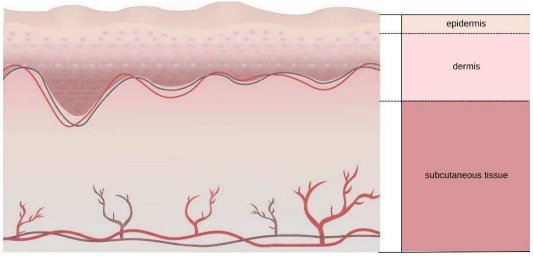


Fig. 2. Skin tissue stratification.

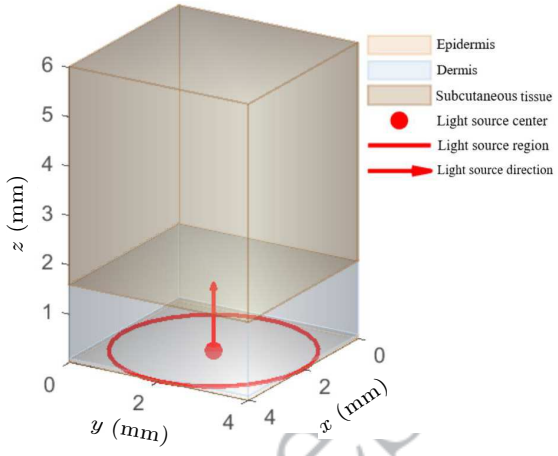


Fig. 3. Skin model structure.

2.2. DPL bioheat transfer equation and arrhenius thermal damage criterion

This paper uses the dual-phase-lag (DPL) bioheat transfer model to capture potential non-Fourier thermal responses under short-pulse heating. This model modifies Fourier's law by introducing two relaxation times, which are the heat flux relaxation time and the temperature gradient relaxation time. Combining this modified law with the energy conservation equation yields the governing bioheat equation

$$\nabla\cdot(k\nabla T) + \tau_T \frac{\partial}{\partial t}[\nabla\cdot(k\nabla T)] + Q(\boldsymbol{r},t) + \tau_q \frac{\partial Q(\boldsymbol{r},t)}{\partial t} = \rho_{\mathrm{c}}\left(\frac{\partial T}{\partial t} + \tau_q \frac{\partial^2 T}{\partial t^2}\right).$$

When $\tau_T = \tau_q = 0$, the model simplifies to the classic Pennes bioheat equation. The blood perfusion term follows the Pennes formulation. Here, ρ_{c} denotes tissue volumetric heat capacity, $Q(r,t) = \omega_{\mathrm{b}}(T)\rho_{\mathrm{b}}c_{\mathrm{b}}(T_{\mathrm{b}} - T) + Q_{\mathrm{met}} + Q_{\mathrm{ext}}$, $\rho_{\mathrm{b}}c_{\mathrm{b}}$ is blood volumetric heat capacity, ω_{b} stands for blood perfusion rate, T_{b} is arterial blood temperature, Q_{met} signifies metabolic heat generation, and Q_{ext} is the laser heat source. The initial values of thermal conductivity k, volumetric heat capacity ρ_{c}, and perfusion-related ω_{b} parameters, along with stratified parameters, are shown in Table 3.

Thermal damage is characterized using the Arrhenius model.[34] The damage integral Ω is calculated from the temperature history (Eq. (1)):

$$\Omega(t) = \int_0^t A\,\mathrm{e}^{-\frac{\Delta E}{RT(t)}}\,\mathrm{d}t, \tag{1}$$

where $A = 3.14 \times 10^{98}$ s^{-1} is the frequency factor, $\Delta E = 6.28 \times 10^5$ $\mathrm{J\cdot mol^{-1}}$ is the activation energy, and $R = 8.314$ $\mathrm{J\cdot mol^{-1}\cdot K^{-1}}$ is the gas constant. Irreversible damage occurrence and its spatial extent are defined by reaching a specified critical threshold value.

CPL Online In-Press

2.3. Heat transfer model and boundary conditions

2.3.1. The 1D and 2D model forms

The 1D model considers heat transfer only along the depth direction (z-axis). Its spatial operator is therefore $\nabla = \partial/\partial z$. The 2D model accounts for both lateral heat diffusion and depth-wise conduction within the y–z plane, using the spatial operator $\nabla = (\partial/\partial y, \partial/\partial z)$. Therefore, the 1D and 2D heat transfer models are respectively as follows (Eqs. (2) and (3)):

$$\begin{aligned}&(1+\tau_q^j(T_\mathrm{s})\frac{\partial}{\partial t})\Big[\rho_\mathrm{s}^j(T_\mathrm{s})c_\mathrm{s}^j(T_\mathrm{s})\frac{\partial T_\mathrm{s}^j}{\partial t}-\omega_\mathrm{b}^j(T_\mathrm{s})\rho_\mathrm{b}c_\mathrm{b}(T_\mathrm{b}-T_\mathrm{s}^j)\\&-Q_\mathrm{met}^j-Q_\mathrm{ext}^j\Big]=\left(1+\tau_T^j(T_\mathrm{s})\frac{\partial}{\partial t}\right)\nabla[k_\mathrm{s}^j(T_\mathrm{s})\nabla T_\mathrm{s}^j],\\&(j=1,2,3),\end{aligned}\tag{2}$$

$$\begin{aligned}&\left(1+\tau_q^j(T_\mathrm{s})\frac{\partial}{\partial t}\right)\left[\rho_\mathrm{s}^j(T_\mathrm{s})c_\mathrm{s}^j(T_\mathrm{s})\frac{\partial T_\mathrm{s}^j}{\partial t}-\omega_\mathrm{b}^j(T_\mathrm{s})\rho_\mathrm{b}c_\mathrm{b}(T_\mathrm{b}-T_\mathrm{s}^j)\right.\\&\left.-Q_\mathrm{met}^j-Q_\mathrm{ext}^j\right]=\left(1+\tau_T^j(T_\mathrm{s})\frac{\partial}{\partial t}\right)\frac{\partial}{\partial z}\left[k_\mathrm{s}^j(T_\mathrm{s})\frac{\partial}{\partial z}T_\mathrm{s}^j\right]\\&+\left(1+\tau_T^j(T_\mathrm{s})\frac{\partial}{\partial t}\right)\frac{\partial}{\partial y}\left[k_\mathrm{s}^j(T_\mathrm{s})\frac{\partial}{\partial y}T_\mathrm{s}^j\right],\quad(j=1,2,3).\end{aligned}\tag{3}$$

Here, T_s represents instantaneous temperature, with j subscripts indicating specific skin layers. The temperature dependencies of the thermal conductivity, volumetric heat capacity, and perfusion-related parameters are taken in the forms of Eqs.(4), (5), and (6), respectively. Heat flux relaxation time and temperature gradient relaxation time are determined using a theoretical method proposed by Zhang *et al.*,[35] which relates vascular geometry to thermal relaxation times.[36] Subsequent comparative calculations will either include or ignore their temperature dependence to quantify simplification errors. Thermal parameters adopt these forms[37]

$$k(T_\mathrm{s})=A_k(T_\mathrm{s}-T_\mathrm{so})^{M_k}+k_0,\quad T_\mathrm{so}\le T_\mathrm{s}\le T_\mathrm{sm},\tag{4}$$

$$\rho c(T_\mathrm{s})=A_{\rho c}(T_\mathrm{s}-T_\mathrm{so})^{M_{\rho c}}+\rho_0 c_0,\quad T_\mathrm{so}\le T_\mathrm{s}\le T_\mathrm{sm}.\tag{5}$$

Here A_k, M_k, $A_{\rho c}$, and $M_{\rho c}$ are constants, and each layer is consistent, as shown in Table 2. k_0 and $\rho_0 c_0$ represent the thermal conductivity and volumetric heat capacity of each layer, respectively, as shown in Table 3. Blood perfusion is treated as[38]

$$\omega_\mathrm{b}(T_\mathrm{s})=\omega_\mathrm{b}(T_0)\,\mathrm{e}^{\frac{T_\mathrm{s}-T_0}{T_0}}.\tag{6}$$

The temperature-dependent parameter coefficients of each layer, as well as the initial values of thermophysical properties for each skin layer and blood, are listed in Tables 2 and 3, respectively.

Table 2. Temperature-dependent parameter coefficients for each layer.[37]

Parameter	A_k	M_k	$A_{\rho c}$	$M_{\rho c}$
Value	0.270×10^{-3}	1.642	0.541×10^{3}	1.823

Table 3. Initial values of thermophysical properties for each skin layer and blood.[24]

Parameter	Blood	Epidermis	Dermis	Subcutaneous tissue
Thermal conductivity $[T(r,0)=T_0]$	0.5	0.235	0.445	0.185
Volumetric heat capacity $[T(r,0)=T_0]$	3996200	4284000	3682800	2621700
Blood perfusion rate $[T(r,0)=T_0]$	–	0	0.00125	0
Initial temperature $[T(r,0)=T_0]$			37	
Thickness $[T(r,0)=T_0]$	–	0.1	1.5	4.4
Metabolic heat production $[T(r,0)=T_0]$	–	368.1	368.1	368.3

This paper further extends the heat transfer model to multi-dimensional skin tissues, and incorporates temperature-dependent thermal property parameters. It constructs 1D and 2D heat transfer models to investigate the dimensional effects of different parameters, as well as studies the temperature sensitivity of thermal property parameters under different dimensions by adding switches for temperature dependency of various parameters.

2.3.2. Initial conditions, boundary conditions, and interlayer interface conditions

The initial condition is $T(r,0)=T_0$. For the DPL equation containing a second-order time derivative, an initial heating rate is also specified $\partial T/\partial t|_{t=0}=0$. External boundaries employ adiabatic conditions $q\cdot n=0$, where is the outward unit normal vector. For the 1D case, this applies at $z=0$ and $z=L$. In the 2D case, it applies at $z=0,L$ and $y=0,L$.

Interlayer interfaces satisfy temperature continuity and heat flux continuity: $T_1=T_2$, $k_1\frac{\partial T_1}{\partial z}=k_2\frac{\partial T_2}{\partial z}$. Here, subscripts 1 and 2 denote adjacent layers on either side of the interface, ensuring continuous heat flux across layers.

2.3.3. Numerical discretization and stability explanation

Governing equations are discretized using a finite difference method and solved via explicit time stepping. The specific solution scheme is detailed in Appendix A. To ensure stability of the explicit difference scheme, time step Δt must satisfy the constraint[39]

$$\Delta t\le\min\left(0.1\cdot\frac{\Delta x^2}{2\alpha_\mathrm{min}},0.1\cdot\frac{\Delta y^2}{2\alpha_\mathrm{min}}\right),$$

CPB Online In-Press

where $\alpha_{\min} = \min(k/\rho c)$ is the minimum thermal diffusivity. Spatial grids and time steps are selected based on stability constraints. All comparative models in this study use identical grid and time step settings. The 1D case meets depth-wise stability requirements, while the 2D case must satisfy both lateral and depth-wise requirements. These settings ensure that the differences between the models stem primarily from the treatment of temperature dependence or model dimensionality (1D/2D) rather than numerical errors.

2.4. Thermal damage sensitivity analysis: reference model and error metric

Targeting the simulation results of accumulated thermal damage, three types of error calculation methods were designed. These methods are used to quantify the differences between three models — only specific heat temperature dependence, only thermal conductivity temperature dependence, and full constant parameters with the reference model — and the fully temperature-dependent model.

(i) Spatiotemporal L_2-norm error

Using the thermal damage parameter Ω from the fully temperature-dependent model as the benchmark, compute the difference between Ω from each comparative case and this benchmark. A global error is characterized by the L_2-norm of the spatiotemporal integral:[40]

$$E_{L_2} = \frac{\sqrt{\int_t \int_x (\Omega_c - \Omega_b)^2 \mathrm{d}x\mathrm{d}t}}{\sqrt{\int_t \int_x \Omega_b^2 \mathrm{d}x\mathrm{d}t}}.$$

Here, Ω_c is the thermal damage parameter from a comparative case, and Ω_b is from the benchmark case. The integration domain covers the entire simulated spatial range and time range t. This metric reflects the overall prediction bias in thermal damage across the global domain. It eliminates scale differences, thereby facilitating comparison across different scenarios.

(ii) Maximum thermal damage error

This metric captures the extreme deviation between two models across all spatial and temporal points:

$$E_{\max} = \max(|\Omega_c - \Omega_b|).$$

It takes the maximum absolute difference in Ω at all spatial points z and time points t. This characterizes the most severe local error a simplified model might introduce in predicting thermal damage.

(ii) Critical damage time error

This quantifies the prediction bias in the time when irreversible damage occurs.

$$\Delta t = t_c - t_b.$$

Here, t_c is the time when the target location (e.g., the basal layer) first reaches the critical value in the comparative case, and t_b is the corresponding time in the benchmark case.

3. Numerical simulation results and analysis

3.1. Model validation

To verify the correctness of the model constructed in this study and the numerical solution method, the same physical model and parameter settings as in Ref. [19] were adopted. Simulations of the temperature change process on the tissue surface after laser irradiation were conducted under two scenarios, non-parametric temperature dependence (TIP) and parametric temperature dependence (TP). The results were then compared with those from the literature. Figure 4 shows the comparison results. In the figure, S-TIP represents the non-temperature-dependent parameter model of this study, S-TP represents the temperature-dependent parameter model of this study, W-TIP represents the non-temperature-dependent parameter model of Wang *et al.*, and W-TP represents the temperature-dependent parameter model of Wang *et al.* Figure 4 shows that when both parameter settings are applied, the temperature curves obtained from the simulations in this study are highly consistent with the literature results, while the differences between them remain within a reasonable error range.

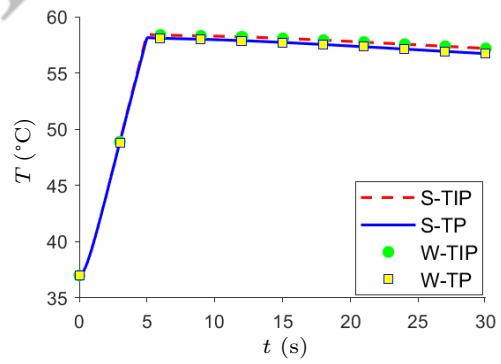


Fig. 4. Comparison between the simulation results of this study and those of Wang *et al.*

3.2. Optical heat source and temperature response: 1D benchmark and key time scales

Initial laser energy deposition within tissue primarily governs subsequent temperature field evolution. As Fig. 5 illustrates, a Gaussian beam produces maximum light power density at the irradiation center, with rapid decay along the radial direction. The epidermis has a lot of melanin, so it absorbs much more than other layers. Consequently, it becomes the dominant layer for energy absorption. The dermis primarily absorbs light via hemoglobin, but its lower absorption coefficient results in relatively moderate energy deposition. Subcutaneous tissue lacks strong absorbers, leading to the weakest light energy absorption. This stratified light energy distribution establishes a spatial foundation for the ensuing temperature field and damage zone. Initial laser energy deposition in tissue serves as the heat source input for subsequent temperature and thermal damage simulations.

CPB Online In-Press

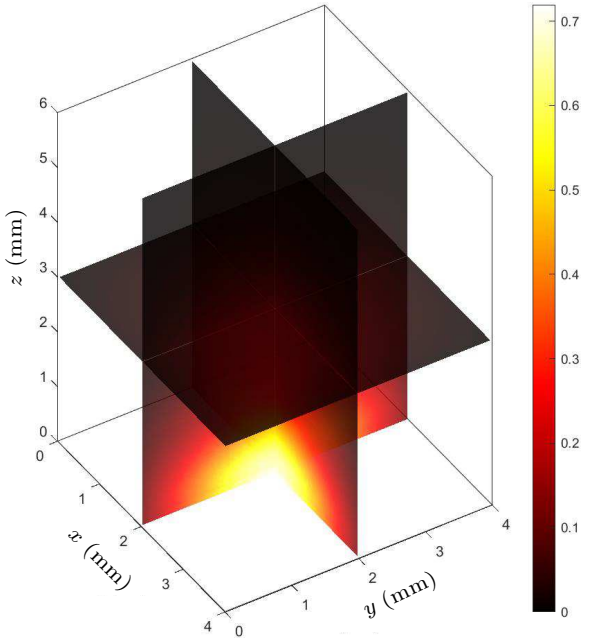


Fig. 5. Interactive 3D slicing of light power density distribution in units of W/mm^2.

After obtaining the three-dimensional optical energy distribution, extract the light power density distribution data along the line $y = 1$ mm, $x = 1$ mm and couple it with the one-dimensional DPL equation. With a light source time of 5 s and a simulation duration of 30 s, the temperature change curve of the tissue surface over time can be obtained. Figure 6 clearly reveals typical stages of skin surface temperature change during laser thermotherapy. In the figure, TP denotes the model considering temperature dependence for all thermophysical parameters, serving as the benchmark. V-TP indicates only volumetric heat capacity varies with temperature. k-TP indicates only thermal conductivity varies with temperature. TIP indicates all thermophysical parameters are held constant. (For conciseness in subsequent figures and tables, these abbreviations are maintained: TP for fully temperature-dependent model, V-TP for only volumetric heat capacity temperature-dependent, k-TP for only thermal conductivity temperature-dependent, and TIP for fully temperature-independent model. Their definitions remain consistent with this section.)

During the initial irradiation phase ($t < 2$ s), the temperature rises rapidly in an approximately linear manner. The laser energy input rate significantly exceeds the heat dissipation rate caused by tissue thermal diffusion and blood perfusion. At $t = 5$ s, the temperature is highest, which means the heat coming in and the heat going out are balanced.

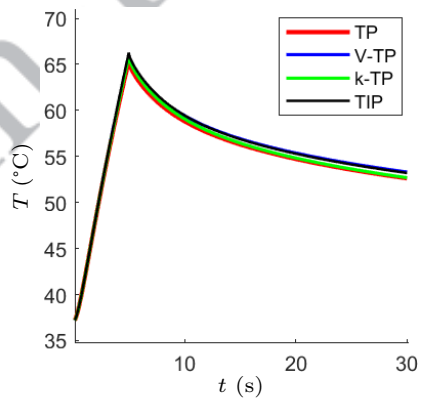


Fig. 6. Variation of tissue surface temperature with time under different parameter models.

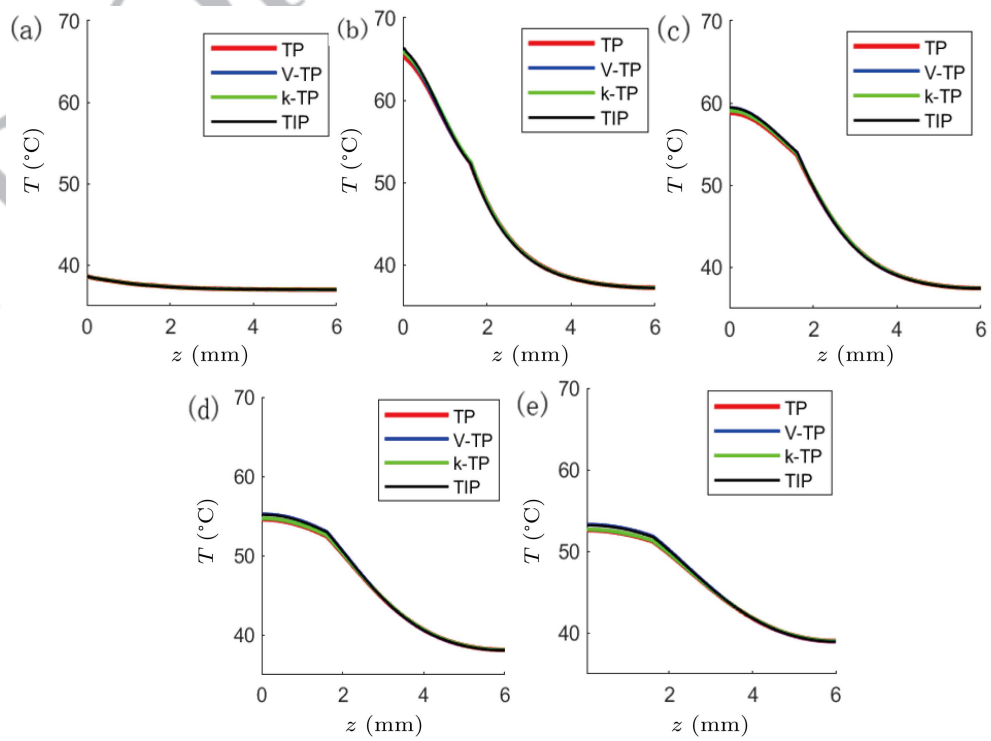


Fig. 7. Radial distribution of temperature at different time points: (a) $t = 0.5$ s, (b) $t = 5$ s, (c) $t = 10$ s, (d) $t = 20$ s, (e) $t = 30$ s.

CPL Online In Press

Subsequently, the temperature enters a phase of gradual decline. This occurs because sustained cooling from blood perfusion begins to dominate. It also reflects the lagging characteristic of heat propagation inherent in the DPL model.

Figure 7 analyzes temperature distributions along tissue depth at different times, revealing a distinct heat wave propagation process.

(i) $t = 0.5$ s, Fig. 7(a): The high-temperature zone is strictly confined to superficial layers. This demonstrates a finite speed effect in heat propagation at very short time scales, indicating significant non-Fourier behavior.

(ii) $t = 5$ s, Fig. 7(b): The heat wave front has penetrated to approximately 1.5 mm depth, covering most of the dermis. Epidermal temperature remains highest, but the temperature rise in the upper dermis is already considerable.

(iii) $t = 10$ s to 30 s, Figs. 7(c)–7(e): Heat further diffuses into the subcutaneous tissue. However, due to blood perfusion in this layer and the tissue's own thermal conduction, the temperature amplitude decreases significantly with increasing depth. The distribution curve becomes smoother.

This entire evolution process shows that the DPL model effectively captures the transition from non-Fourier effects to Fourier-like diffusion during laser heating.

3.3. Dimensional effect: 2D temperature field and spatial propagation of thermal damage

Built on the 1D model that only accounts for radial (z-axis) heat transfer, the 2D model is extended to the y–z plane and incorporates the transverse thermal diffusion effect. Optical power density distribution data on the plane $y = 1$ mm from Fig. 5 was coupled with the 2D DPL equation. The light source duration remains 5 seconds, and the simulation duration is 30 seconds. Figure 8 shows the dynamic evolution of the tissue temperature field within the y–z plane under laser irradiation. Unlike the 1D model, which only shows monotonic variation along depth, the 2D temperature field displays distinct spatial gradients. High-temperature regions decrease concentrically from the irradiation center towards the periphery and deeper layers. During initial irradiation ($t \leq 5$ s), energy deposition concentrates in superficial layers. Longitudinal diffusion is weak, causing rapid temperature rise at the center and forming a localized hot core. Over time, longitudinal heat diffusion increases significantly. Heat spreads from the hot core to surrounding tissue, which slows the central temperature rise rate. Temperature distribution across planes at the same depth becomes more uniform. In later stages, combined cooling from blood perfusion and bi-directional heat diffusion leads to a uniform temperature decline across the entire region.

The bi-directional diffusion mechanism captured by the 2D model creates a more complex and realistic thermal damage response scenario compared to the 1D model. Thermal damage accumulation is calculated via the Arrhenius equation, which also exhibits two-dimensional spatial expansion that can be seen in Fig. 9 (TDD stands for thermal damage distribution). The damage zone does not extend linearly

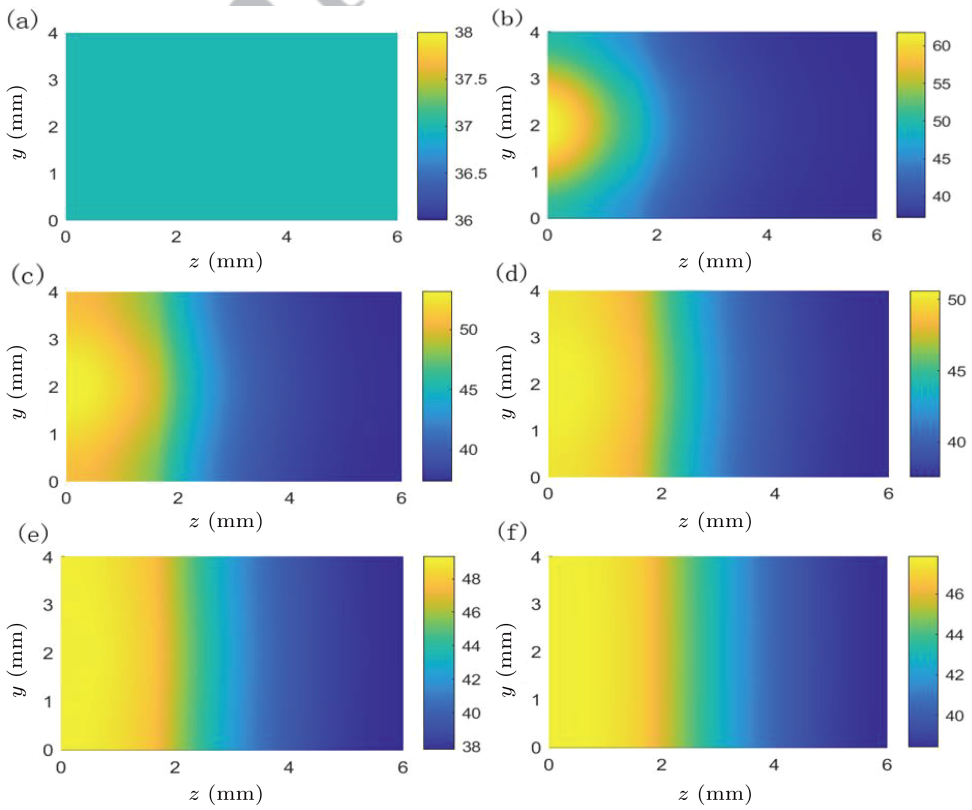


Fig. 8. 2D temperature distribution results: (a) $t = 0$ s, (b) $t = 5$ s, (c) $t = 10$ s, (d) $t = 15$ s, (e) $t = 20$ s, (f) $t = 30$ s.

CPL Online In-Press

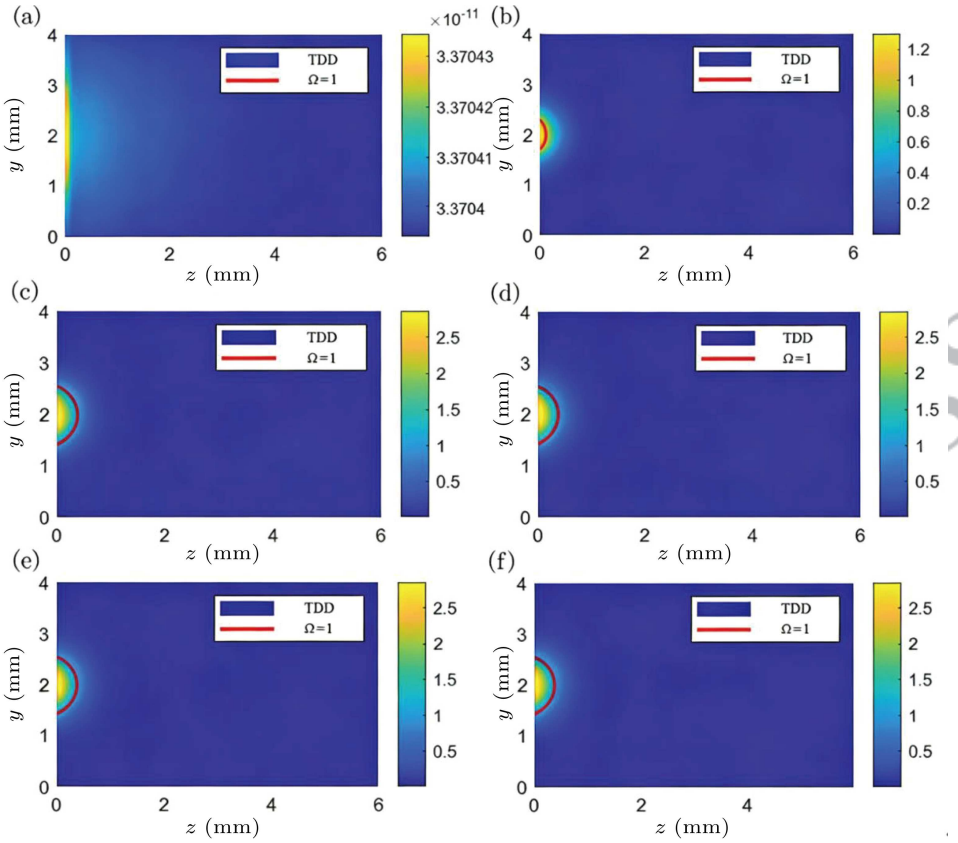


Fig. 9. 2D thermal damage distribution results: (a) $t = 0$ s, (b) $t = 5$ s, (c) $t = 10$ s, (d) $t = 15$ s, (e) $t = 20$ s, (f) $t = 30$ s.

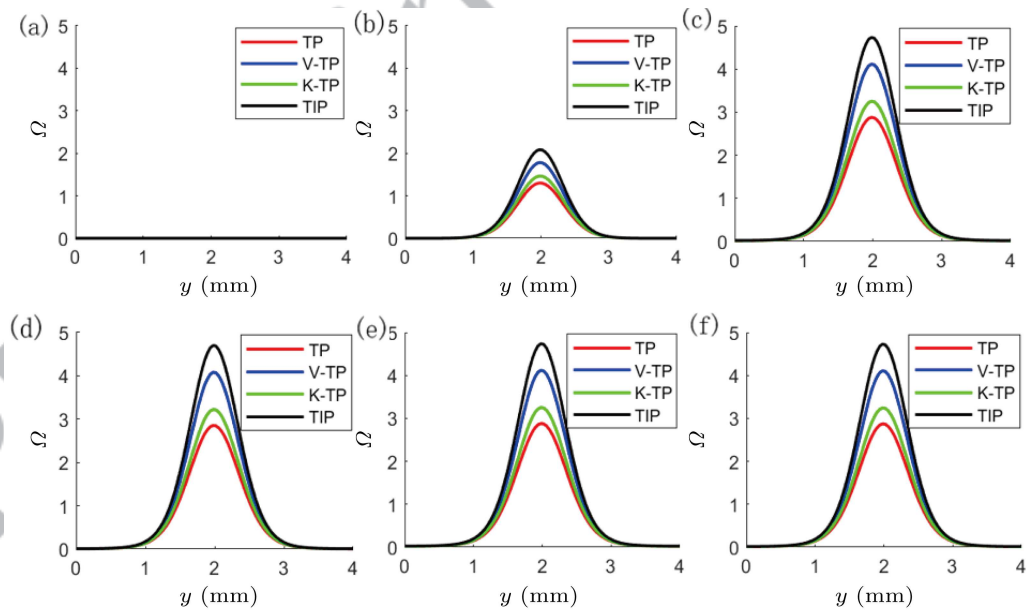


Fig. 10. Temporal variation of surface thermal damage: (a) $t = 0$ s, (b) $t = 5$ s, (c) $t = 10$ s, (d) $t = 15$ s, (e) $t = 20$ s, (f) $t = 30$ s.

downward as predicted by the 1D model. Instead, it expands laterally and radially in a near-circular shape. The moving trajectory of the critical damage boundary ($\Omega = 1$) clearly shows that the damage front penetrates the dermis laterally while its lateral extent continuously expands. It provides a basis for judging skin surface thermal damage scale. Meanwhile, this damage pattern implies that actual treatments produce surface damage areas that are unpredictable with a 1D model.

Extending the model to 2D introduces the lateral dimension, which corresponds to the skin tissue surface. This allows assessment of how different temperature-dependent thermophysical parameters affect surface thermal damage. Figure 10 shows the lateral distribution of thermal damage accumulation along the skin surface (y-direction) at a specific time. Comparing curves from the fully temperature-dependent benchmark model against three others allows quantitative evaluation of

their impact on predicting the lateral extent of the damage width ($\Omega \geq 1$). All comparative models predict a larger damage width than the benchmark. This indicates ignoring temperature dependence systematically overestimates lateral damage extension. The fully fixed parameter model shows the most significant overestimation, with its $\Omega \geq 1$ zone extending farthest laterally. Figure 11 and Table 4 further present the maximum irreversible thermal damage width on the skin surface for different models; the fully fixed parameter model shows the greatest overestimation.

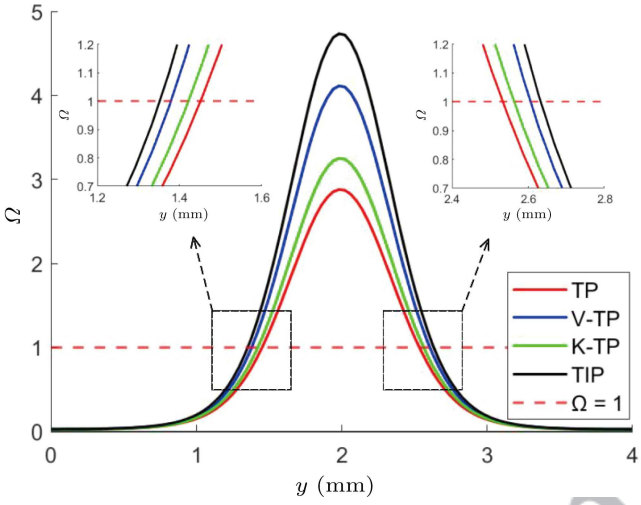


Fig. 11. 2D surface thermal damage distribution map at the final time point.

Table 4. Lateral damage width (along y-axis) at the skin surface ($z = 0$) when accumulated thermal damage equals 1 at the final time point in different 2D models.

	TP	V-TP	k-TP	TIP
Line width (mm)	1.05	1.17	1.09	1.25

3.4. Temperature-dependent parameter sensitivity and model simplification

Table 5 shows that when the 1D model is considered and compared with the benchmark model, all simplified models exhibit systematic biases in their predictions, which are characterized by higher maximum temperatures and earlier critical damage times. This is mainly because the temperature dependence of the parameters is ignored, which leads to a larger temperature response predicted by the model. Among them, the fully fixed parameter model shows the greatest deviation. Its peak temperature is about 1 °C higher and its critical damage time is 0.1 s earlier than the benchmark. In clinical applications, this could cause misjudgment of treatment dosage and safety margins. Table 6 shows that the model with k-TP has a smaller L2 error. This indicates that thermal conductivity's temperature dependence has a more significant impact on overall thermal damage prediction. From a theoretical perspective, thermal conductivity directly governs the rate of heat diffusion within biological tissues by determining the thermal flux response under temperature gradients. This core process controls the spatiotemporal evolution of the temperature field, thereby dictating the extent of cumulative thermal injury. In contrast, volumetric heat capacity primarily modulates thermal inertia, influencing only the rate of temperature change within tissues rather than the fundamental spatial diffusion of heat. The maximum error metric also reveals a smaller local deviation for the k-TP model, further supporting its dominant role. Regarding parameter sensitivity, within the 1D framework and given parameters, the temperature dependence of thermal conductivity contributes slightly more to overall thermal damage prediction error than volumetric heat capacity. This highlights the importance of accurately characterizing the thermal conductivity-temperature relationship when building bioheat models.

Table 5. Comparison of maximum temperature of accumulated thermal damage and time to reach critical thermal damage under 1D different temperature-dependent parameter settings.

	TP	V-TP	k-TP	TIP
Highest temperature (°C)	65.35	65.82	65.76	66.35
Reach critical thermal injury time (s)	4.33	4.27	4.28	4.23

Table 6. Spatiotemporal errors of thermal damage integral Ω between each simplified 1D model and the benchmark model.

Error metric	V-TP	k-TP	TIP
Spatiotemporal L_2 error	0.40	0.30	0.64
Maximum error	17.49	11.89	28.19

The one-dimensional results of this paper provide a clear perspective on the fundamental patterns of parameter sensitivity. The results lay the foundation for subsequent, more complex 2D model analysis and optimization of the model's clinical applicability.

For the 2D model analysis, Fig. 11 visually compares the spatial morphology of skin surface thermal damage distribution at the simulation end time under four different settings. Combined with quantitative lateral width data in Table 4, differences between model predictions become clear. The TP model predicts the smallest damage width (1.05 mm). The k-TIP model follows (1.09 mm). The V-TIP model is larger (1.17 mm). The TIP model predicts the greatest width (1.25 mm). The impact of each parameter on damage width is analyzed as follows.

(i) V-TIP: The increase in damage width is primarily attributed to the overestimation of the overall energy accumulation process, which leads to more regions reaching the damage threshold. However, its expansion morphology is basically similar to that of the reference model, with relatively consistent edge gradient changes.

(ii) k-TIP: Increased damage width is more evident in the movement of the damage edge. Fixing thermal conductivity as a constant reduces the resistance to heat diffusion from high-temperature zones to surrounding tissue. Heat disperses lat-

CPB Online In-Press

erally more easily, pushing the damage threshold further outward. Therefore, thermal conductivity has a more direct and significant impact on damage width.

(iii) TIP: Increased damage width results from superimposing both effects described above. Due to parameter coupling, its expansion range is most severe.

In clinical laser therapy practice, a prediction error of approximately 0.2 mm in overestimating the transverse lesion width significantly impacts the precise planning of treatment boundaries. Overly conservative safety margins may damage more healthy tissue or limit therapeutic efficacy in delicate areas such as the face. Accumulated errors across multiple treatments may further compromise overall treatment layout and healing outcomes. Therefore, incorporating the temperature sensitivity of thermophysical parameters into treatment planning is crucial for enhancing clinical precision and safety.

Figure 12 shows curves of thermal damage area (the area where $\Omega \geq 1$ in the 2D models) evolving over time. All simplified models that consider temperature dependence for some parameters — V-TP, k-TP, and TIP — predict larger thermal damage areas than TP. This indicates that ignoring the temperature dependence of thermophysical parameters systematically overestimates both lateral and radial damage extension. Clinically, this could also lead to overestimation of treatment zones and safety margins. Among them, the completely fixed parameter model predicts the largest damage area, and the deviation from the benchmark model increases gradually over time, indicating a significant bias in the parameter constant hypothesis when predicting cumulative damage.

Table 7 presents errors in the spatiotemporal variation of the $\Omega \geq 1$ area for different models in Fig. 12, compared to the benchmark. Regarding the spatiotemporal L2-norm error, the V-TP model has the smallest error. This suggests that holding volumetric heat capacity constant has a relatively limited impact on overall damage area prediction in this 2D model. In contrast, the k-TP model has a noticeably higher L2 error, indicating that thermal conductivity's temperature dependence more significantly affects damage scale. The TIP model has the largest L2 error, substantially higher than the other two. This further reveals that a nonlinear coupling effect exists between the temperature dependencies of multiple thermophysical parameters. Ignoring them simultaneously significantly amplifies prediction uncertainty.

Analysis of maximum error shows a consistent trend with L2 error. The k-TP model has the smallest maximum deviation, the V-TP model is next, and the TIP model is largest. This indicates that although each model may exhibit significant local deviations at certain spatiotemporal points, the overall temperature dependence of thermal conductivity remains the dominant factor affecting the prediction accuracy of the damage range.

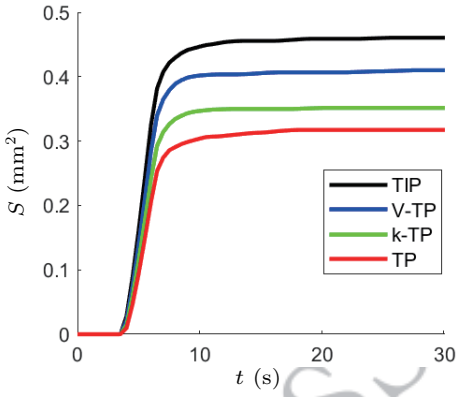


Fig. 12. Area variation of thermal damage greater than 1 in different 2D models.

Table 7. The thermal damage prediction errors of different models in Fig. 12.

Error metric	V-TP	k-TP	TIP
Spatiotemporal L_2 error	0.46	0.19	0.71
Maximum error	1.23	0.37	1.86

4. Conclusion

This paper is based on an improved dual-phase lag (DPL) model that combines Monte Carlo light transport simulation with a finite-difference numerical solution. By using this approach, the evolution of the temperature field and the accumulation of thermal damage in skin tissue under laser irradiation are systematically investigated. It focuses on investigating the impact of the temperature dependence of thermodynamic parameters on prediction results, and conducts parameter sensitivity comparative analysis under 1D and 2D model frameworks. The main conclusions are as follows.

(i) The constructed DPL model successfully captures the non-Fourier heat transfer behavior under short-pulse laser irradiation and exhibits good numerical stability in both 1D and 2D models.

(ii) The coupling effect of multiple parameters is significant; simplifying any single parameter may lead to deviations, and completely ignoring temperature dependence will result in the greatest predictive uncertainty.

(iii) The temperature dependence of thermophysical parameters systematically affects temperature field and thermal damage predictions. Neglecting this dependency leads to overestimation of peak temperatures, expansion of thermal damage zones, and earlier critical damage times. For instance, ignoring the temperature dependence of all parameters results in a 0.2 mm overestimation of lateral damage width and an approximately 0.1-second advance in predicted critical damage time. Among these parameters, the temperature sensitivity of thermal conductivity is the most pronounced.

(iv) Compared to 1D models, 2D models more accurately reflect the spatial expansion morphology of damaged areas by introducing lateral heat diffusion. Research results have

CPB Online In-Press

shown that lateral heat diffusion further amplifies the overestimation of damage range caused by neglecting the temperature dependence of thermal conductivity. This finding highlights the importance of using multi-dimensional models when evaluating the scale of surface damage.

(v) In 1D and 2D models, the temperature dependence of thermal conductivity is a dominant factor affecting the accuracy of thermal damage prediction, with its error contribution being higher than that of volumetric heat capacity. The multi-parameter coupling effect further amplifies the uncertainty of the fully constant assumption.

Although this paper clarifies the core influence laws of the temperature dependence of thermophysical parameters and model dimensionality on the prediction of thermal damage in skin tissue, it provides a theoretical reference for damage prediction in laser thermotherapy. There are still many aspects to be optimized in practical clinical translation and model system improvement. In terms of parameter optimization, a closed-loop optimization system for optical–thermal parameters considering individual tissue differences and the reverse regulation of thermal damage has not been constructed, nor has the global intelligent optimization of multi-parameter coupling been realized. In terms of model simplification, the lack of three-dimensional heat transfer, the idealized assumption of skin sublayers and appendages, and the neglect of multi-physical field coupling lead to a deviation between the model and the actual heat transfer process of biological tissues. In terms of safety boundary definition, a specific threshold system for different tissue layers and damage types has not been established, nor has the prediction error of the model been incorporated into the quantitative design of safety margins. For tissues exhibiting significant anisotropy, the model must be enhanced by incorporating an anisotropic Monte Carlo photon transport model and an anisotropic DPL bioheat transfer equation. These shortcomings will be addressed in subsequent research.

Appendix: Numerical solution

The calculation method adopts the discrete format — finite difference method. The control equation is discretized using an explicit difference scheme, with second-order backward difference in time and second-order central difference in space.

(i) One-dimensional model

Only heat transfer in the thickness direction (z-axis) is considered, and spatial derivatives only contain components in the z-direction.

Time discretization: Let T_i^n be the dimensionless temperature at the n-th time step and i-th grid point. The time step is denoted as Δt, then the first-order and second-order time derivatives are approximated as

$$\frac{\partial T}{\partial t} \approx \frac{T_i^n - T_i^{n-1}}{\Delta t}, \frac{\partial^2 T}{\partial t^2} \approx \frac{T_i^n - 2T_i^{n-1} + T_i^{n-2}}{\Delta t^2}.$$

Space discretization: The spatial step is Δz. The second-order spatial derivative is approximated as

$$\frac{\partial^2 T}{\partial z^2} \approx \frac{T_{i+1}^n - 2T_i^{n-1} + T_{i-1}^{n-2}}{\Delta z^2}.$$

Iteration formula: The discretized temperature update formula for 1D is

$$\begin{aligned} T_i^{n+1} =\ & (2 - \frac{a_2}{a_1}\Delta t)T_i^n - (1 - \frac{a_2}{a_1}\Delta t + \frac{a_3}{a_1}\Delta t^2)T_i^{n-1} \\ & + \frac{b_1}{a_1} \cdot \frac{\Delta t}{\Delta z^2}[(T_{i+1}^n - 2T_i^n + T_{i-1}^n) - (T_{i+1}^{n-1} \\ & - 2T_i^{n-1} + T_{i-1}^{n-1})] + \frac{b_2}{a_1} \cdot \frac{\Delta t^2}{\Delta z^2}(T_{i+1}^n - 2T_i^{n-1} + T_{i-1}^{n-1}) \\ & + Q_i. \end{aligned}$$

Here coefficients a_1, a_2, a_3, b_1, b_2 are calculated from thermophysical parameters and lag times:[19]

$$a_1 = \tau_q \cdot (\rho c),\ \ a_2 = \rho c + \tau_q \cdot \omega_{\mathrm{b}} + \tau_q \cdot \frac{\partial(\rho c)}{\partial t},$$
$$a_3 = \omega_{\mathrm{b}} + \tau_q \cdot \frac{\partial \omega_{\mathrm{b}}}{\partial t},\ \ b_1 = \tau_T \cdot k,\ \ b_2 = k + \tau_T \cdot \frac{\partial k}{\partial t},$$

Q_i is the source term, which includes laser heating and metabolic generation.

(2) Two-dimensional model

This model extends to the y–z plane, requiring spatial derivatives in both directions. The discretization scheme adds y-direction components to the 1D foundation.

Space discretization: The second-order derivative in the y-direction is approximated as

$$\frac{\partial^2 T}{\partial y^2} \approx \frac{T_{i,j+1}^{\mathrm{n}} - 2T_{i,j}^n + T_{i,j-1}^n}{\Delta y^2}.$$

Here, Δy is the spatial step in the y-direction, and $T_{i,j}^n$ is the temperature at grid point (i, j) for time step n.

Iteration formula: The temperature update formula for 2D becomes

$$\begin{aligned} T_{i,j}^{n+1} =\ & (2 - \frac{a_2}{a_1}\Delta t)T_{i,j}^n - (1 - \frac{a_2}{a_1}\Delta t + \frac{a_3}{a_1}\Delta t^2)T_{i,j}^{n-1} \\ & + \frac{b_1}{a_1} \cdot \Delta t \left[\frac{(T_{i+1,j}^n - 2T_{i,j}^n + T_{i-1,j}^n) - (T_{i+1,j}^{n-1} - 2T_{i,j}^{n-1} + T_{i-1,j}^{n-1})}{\Delta z^2} \right. \\ & \left. + \frac{(T_{i,j+1}^n - 2T_{i,j}^n + T_{i,j-1}^n) - (T_{i,j+1}^{n-1} - 2T_{i,j}^{n-1} + T_{i,j-1}^{n-1})}{\Delta y^2} \right] \\ & + \frac{b_2}{a_1} \cdot \Delta t^2 \left(\frac{T_{i+1,j}^{n-1} - 2T_{i,j}^{n-1} + T_{i-1,j}^{n-1}}{\Delta z^2} + \frac{T_{i,j+1}^{n-1} - 2T_{i,j}^{n-1} + T_{i,j-1}^{n-1}}{\Delta y^2} \right) \\ & + Q_{i,j}. \end{aligned}$$

CPB Online In-Press

Acknowledgments

Project supported by the National Natural Science Foundation of China (Grant Nos. 12374440 and 12664073) and the Inner Mongolia University Young Academic Talent Research Start-up Project (Grant No. 10000-23112101/087).

References

[1] Skinner W H, Salimi M, Moran L, Blein-Dezayes I, Mehta M, Mosca S, Vaideanu A G, Gardner B, Palombo F and Schtzlein A G 2025 *J. Phys. Chem. C* **129** 1864
[2] Shimojo Y, Nishimura T, Tsuruta D and Ozawa T 2024 *Sci. Rep.* **14** 20112
[3] Giering K, Minet O, Lamprecht I and Mueller G 1995 *Proceedings of SPIE-The International Society for Optical Engineering,* January, 1995 Los Angeles, United States, p. 45
[4] Mitra K, Kumar S, Vedevarz A and Moallemi M K 1995 *J. Heat Transf.* **117** 568
[5] Antaki P J 2005 *J. Heat Transf.* **127** 189
[6] Tzou D Y 2014 *Macro-to microscale heat transfer: the lagging behavior* (1st edn.) (New York: John Wiley & Sons) p. 21
[7] Tzou D Y 1995 *J. Heat Transf.* **117** 8
[8] Tzou D Y 1995 *J. Thermophys. Heat Transf.* **9** 686
[9] Antaki P J 1998 *Int. J. Heat Mass Transf.* **41** 2253
[10] Pennes H H 1998 *J. Appl. Physiol.* **85** 5
[11] Zhou J, Zhang Y and Chen J K 2009 *Int. J. Therm. Sci.* **48** 1477
[12] Liu K C and Wang J C 2014 *Int. J. Heat Mass Transf.* **70** 621
[13] Diller K R and Pearce J A 1999 *Ann. N. Y. Acad. Sci.* **888** 153
[14] Abraham J P and Sparrow E M 2007 *Int. J. Heat Mass Transf.* **50** 2537
[15] Bhattacharya A and Mahajan R L 2003 *Physiol. Meas.* **24** 769
[16] Lopresto V, Argentieri A, Pinto R and Cavagnaro M 2019 *Phys. Med. Biol.* **64** 105016
[17] Valvano J W, Cochran J R and Diller K R 1985 *Int. J. Thermophys.* **6** 301
[18] Wang Y Z, Lu X Y and Liu D 2023 *Chin. Phys. B* **32** 014401
[19] Wang Y Z, Lu X Y, Wang Z and Zheng W B 2023 *Int. J. Heat Mass Transf.* **213** 124335
[20] Bianchi L, Cavarzan F, Ciampitti L, Cremonesi M, Grilli F and Saccomandi P 2022 *Int. J. Hyperthermia* **39** 297
[21] Arkin H, Xu L X and Holmes K R 2002 *IEEE Trans. Biomed. Eng.* **41** 97
[22] Gautherie M 1990 *Thermal Dosimetry and Treatment Planning* (1st edn.) (Berlin: Springer-Verlag) p. 51
[23] Mongkol V, Rattanadecho P, Preechaphonkul W and Vafai K 2025 *J. Therm. Biol.* **134** 104343
[24] Xu F, Seffen K A and Lu T J 2008 *Int. J. Heat Mass Transf.* **51** 2237
[25] Wilson B C and Adam G 1983 *Med. Phys.* **10** 824
[26] Zhang Y H, Zhu H Z, Dong Y J, Zeng J, Han X P, Ivan A B, Zhang F R, Xu S Y and Wang S 2023 *Chin. Phys. B* **32** 118702
[27] Fang Q and Boas D A 2009 *Opt. Express* **17** 20178
[28] Xu L Z and Li T 2024 *Chin. J. Lasers* **51** 2107104
[29] Nunez A S 2009 *A physical model of human skin and its application for search and rescue* (OH, USA: Air Force Institute of Technology)
[30] Vyas S 2014 *Physics-based Computational Modeling of Human Skin using Machine Learning for Physiological Parameter Estimation* (MD, USA: Johns Hopkins University)
[31] Tuchin V V, Utz S R and Yaroslavsky I V 1994 *Opt. Eng.* **33** 3178
[32] Diller K R and Hayes J 1983 *J. Biomech. Eng.* **105** 300
[33] Nishidate I, Tanaka N, Kawase T, Maeda T, Yuasa T, Aizu Y, Yuasa T and Niizeki K 2011 *J. Biomed. Opt.* **16** 086012
[34] Henriques F C and Moritz A R 1947 *Am. J. Pathol.* **23** 530
[35] Zhang Y 2009 *Int. J. Heat Mass Transf.* **52** 4829
[36] Yuan P 2009 *Int. J. Heat Mass Transf.* **52** 1734
[37] Guntur S R and Choi M J 2020 *Ultrasound Med. Biol.* **46** 1001
[38] Deng Z S and Liu J 2000 *Med. Eng. Phys.* **22** 693
[39] LeVeque R J 2007 *Finite difference methods for ordinary and partial differential equations: steady-state and time-dependent problems* (1st den.) (Philadelphia: Society for Industrial and Applied Mathematics) p. 123
[40] Peng W T and Huang J P 2025 *Pet. Sci.* **22** 1051

CPB Online First